Supplementary Information (SI) for Journal of Materials Chemistry A.
This journal is © The Royal Society of Chemistry 2026

Electronic Supplementary Information

One-Pot Nanocasting of 3D Ordered Bicontinuous Mesoporous Pt-Based Multimetallic Alloys for Efficient Hydrogen Evolution

Chonghan Xia,[1,‡] Junhao Ma,[1,‡] Qihang Chen,[1] Yee Yan Tay,[2] Lydia H. Wong,[1] and Kwan W. Tan[1,*]

Affiliations:

[1]School of Materials Science and Engineering, Nanyang Technological University, Singapore 639798, Singapore.

[2]Facility for Analysis, Characterization, Testing and Simulation, Nanyang Technological University, Singapore 639798, Singapore.

[‡]These authors contribute equally to the work.

*Correspondence: kwtan@ntu.edu.sg

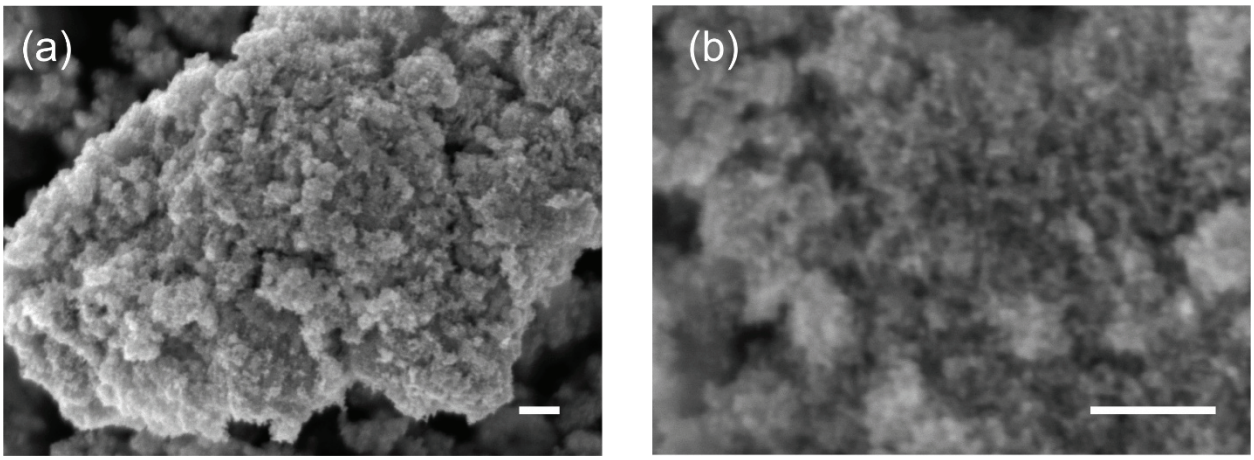

Figure S1. (a,b) SEM images of MMA-1.0-Acid. All scale bars are 100 nm.

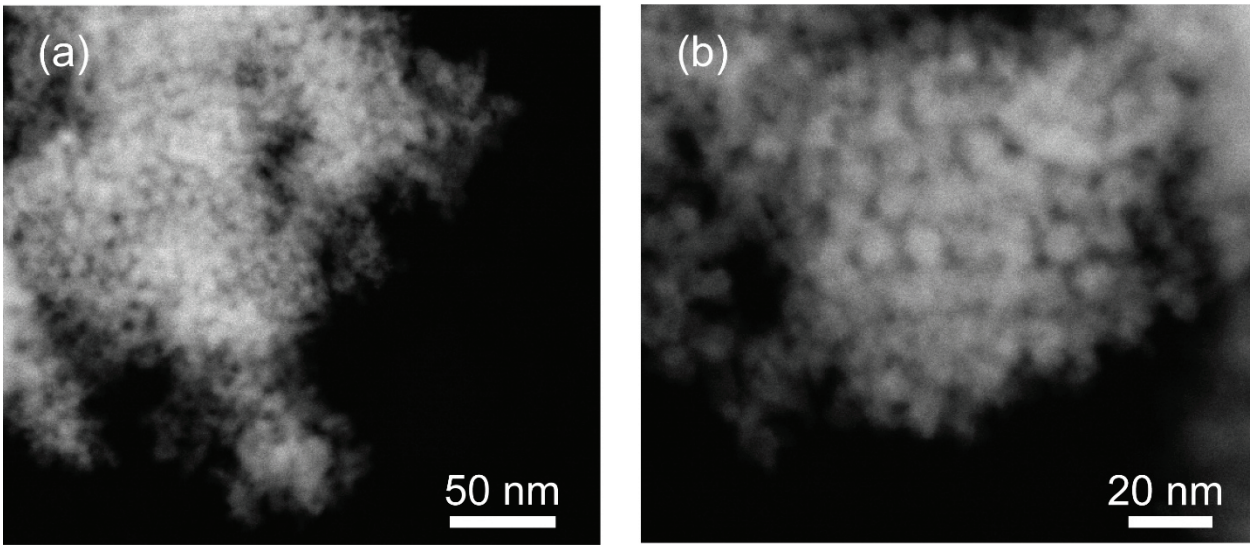

Figure S2. HAADF-STEM micrographs of MMA-0.75-Acid under different magnifications**.**

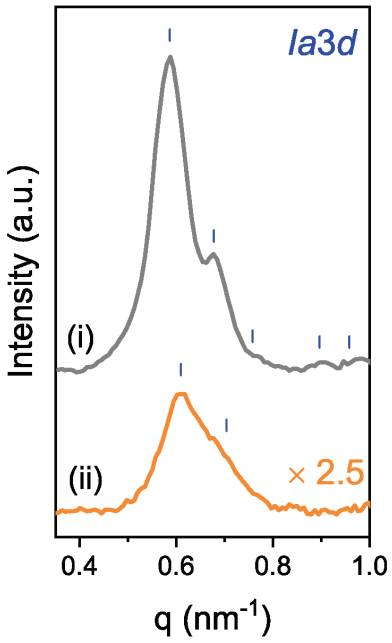

Figure S3. Azimuthally integrated SAXS patterns of the (i) KIT-6 template and (ii) MMA-0.75-Acid sample. The SAXS intensity of the MMA-0.75-Acid pattern is enhanced by a factor of 2.5 for improved clarity. Tick marks indicate the principal reflection and expected higher-order reflections for the $Ia\bar{3}d$ symmetry.

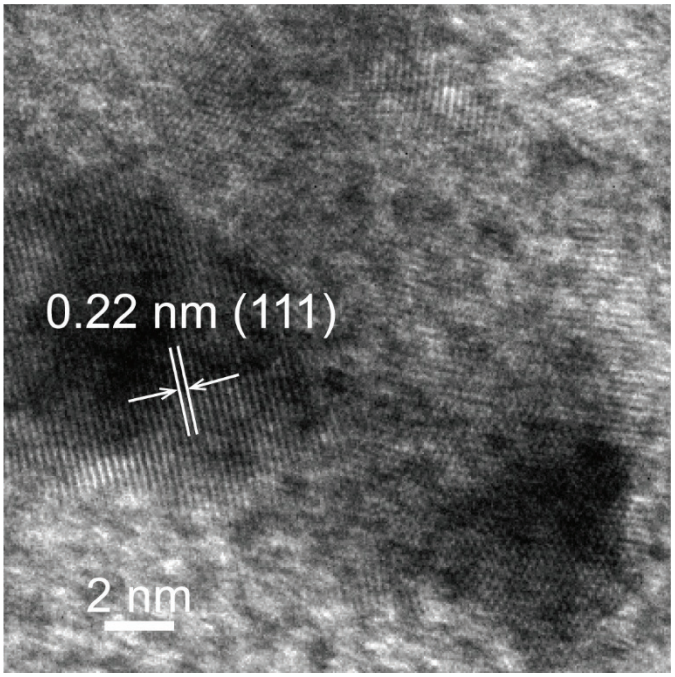

Figure S4. HRTEM micrograph of MMA-0.25-Acid.

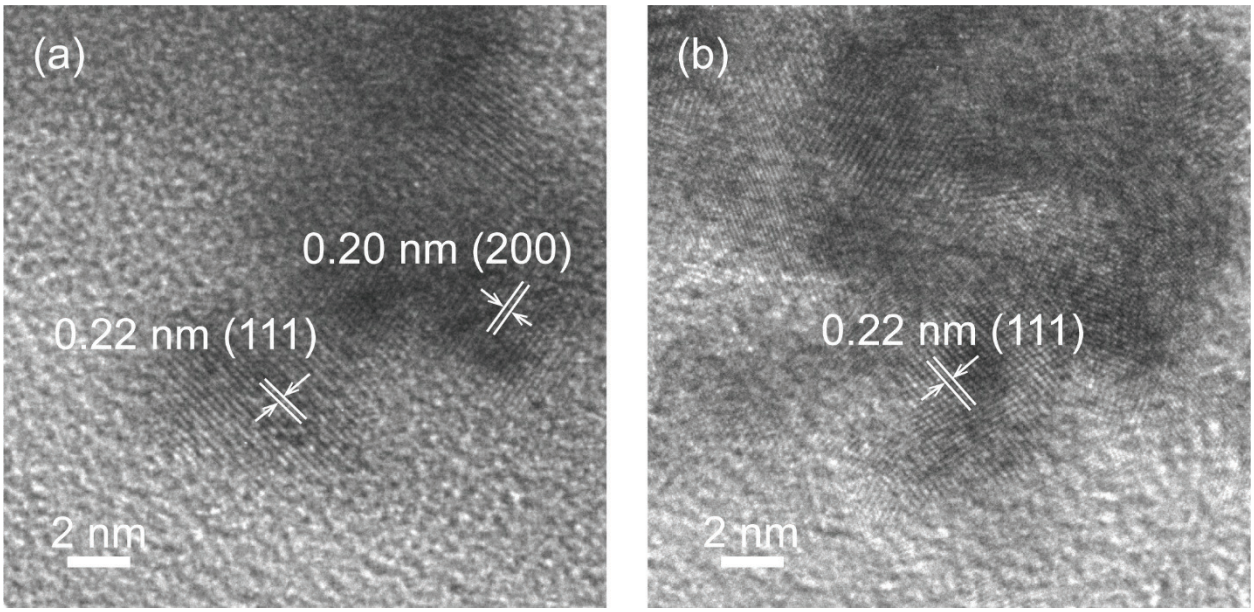

Figure S5. HRTEM images of (a) MMA-0.5 and (b) MMA-0.5-Acid.

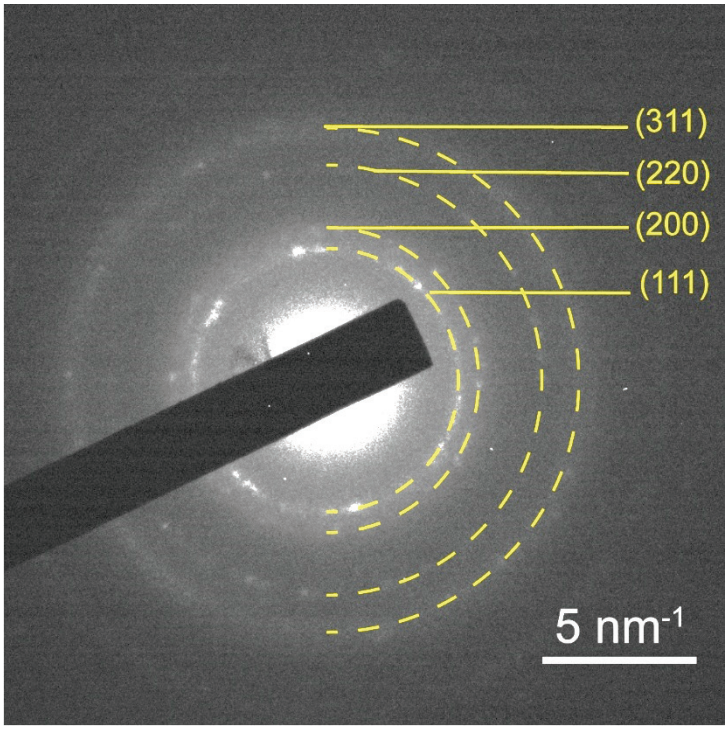

Figure S6. SAED pattern of MMA-0.75-Acid. The diffuse rings are indexed to the fcc reflections (111), (200), (220), and (311), indicating a polycrystalline, single solution fcc structure.

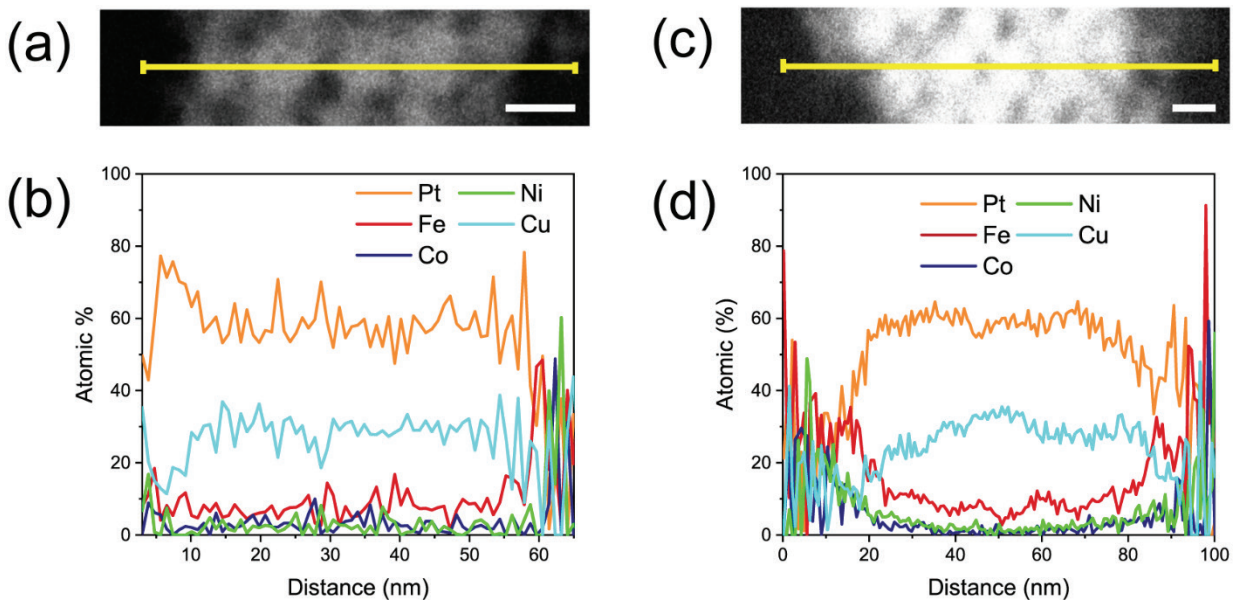

Figure S7. HAADF-STEM and corresponding EDS profiles of as-synthesized samples of (a,b) MMA-0.25 and (c,d) MMA-0.5. All scale bars are 10 nm.

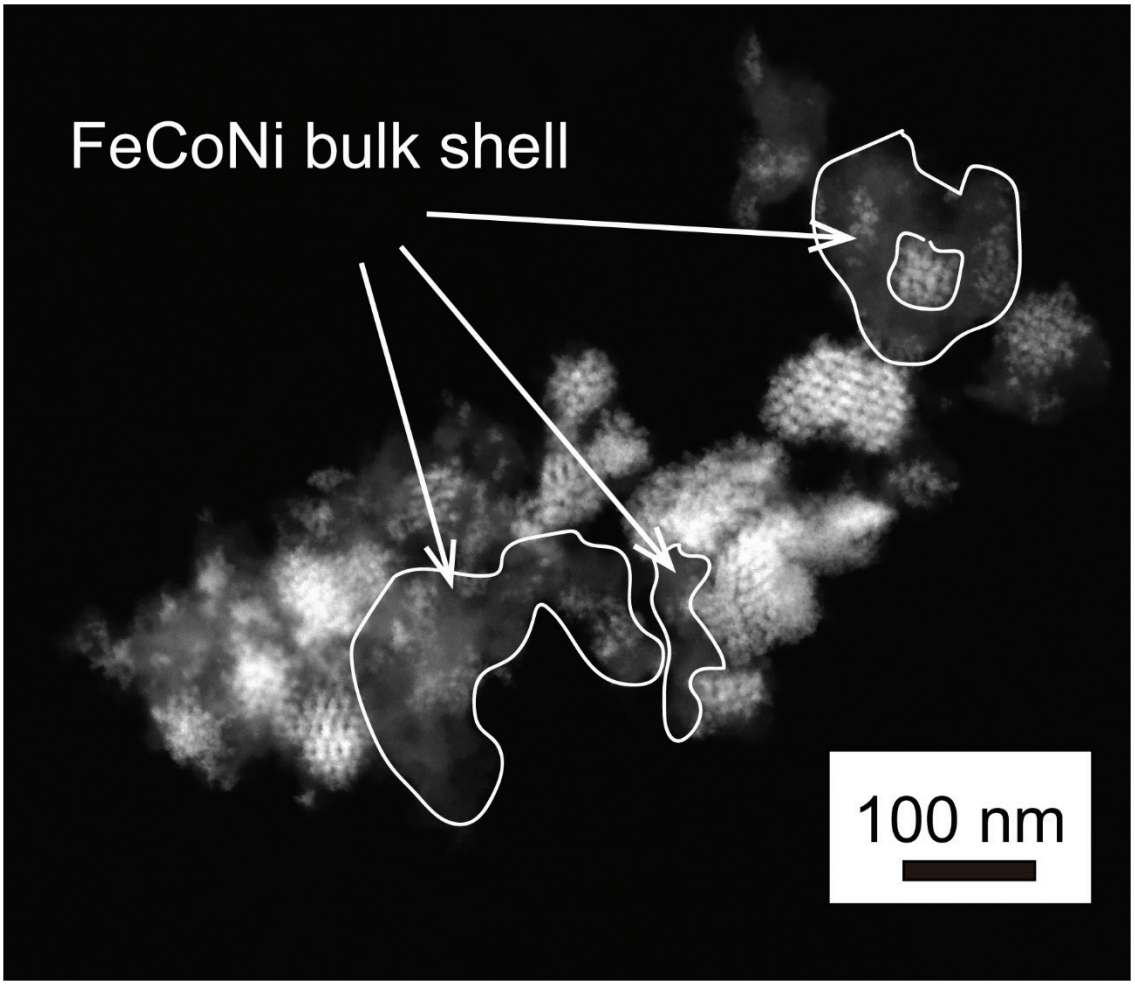

Figure S8. HAADF-STEM image of MMA-0.5 displayed in Figure 2b acquired at lower magnification. The white colored highlighted regions indicate the FeCoNi-enriched bulk shell features formed on the exterior of the mesoporous particle cores.

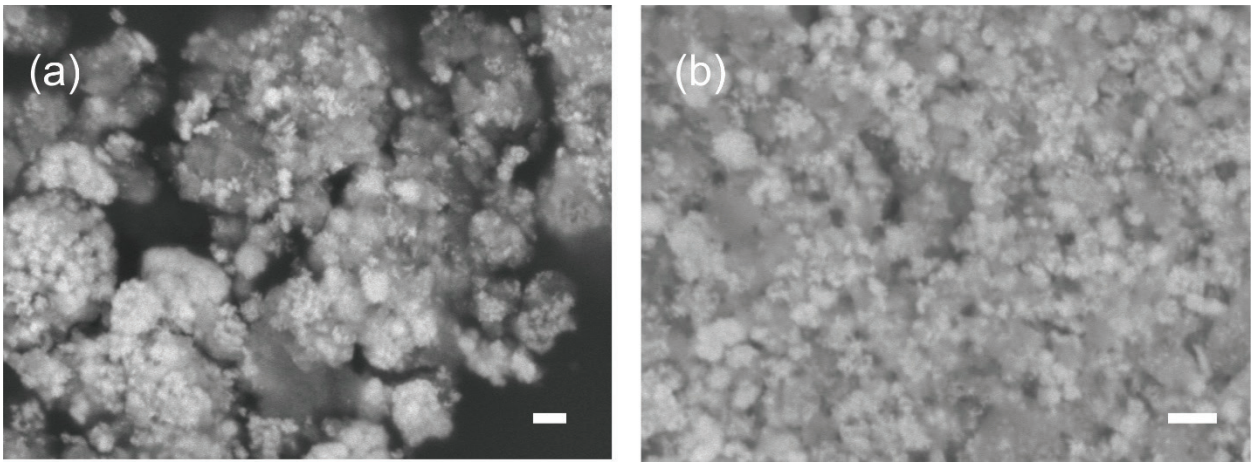

Figure S9. SEM images of MMA-0.75. All scale bars are 100 nm.

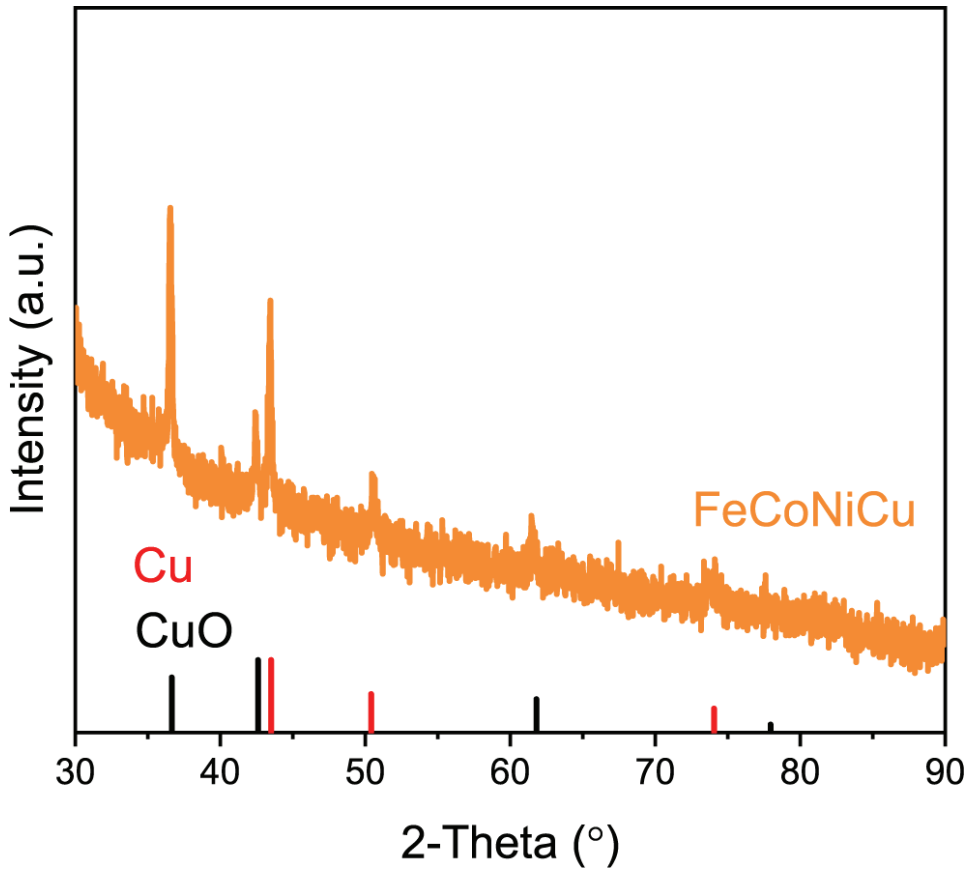

Figure S10. XRD pattern of as-synthesized FeCoNiCu prepared at 0.75 M SBH in the absence of Pt. The diffraction peaks assigned to metallic Cu and CuO, indicating partial oxidation in the Pt-free sample. The emergence of oxide reflections highlights the role of Pt in stabilizing the metallic phase in the mesoporous alloy. Reference XRD peak positions for Cu metal (red, PDF 00-001-1241) and CuO (black, PDF 01-078-0428) are shown for comparison.

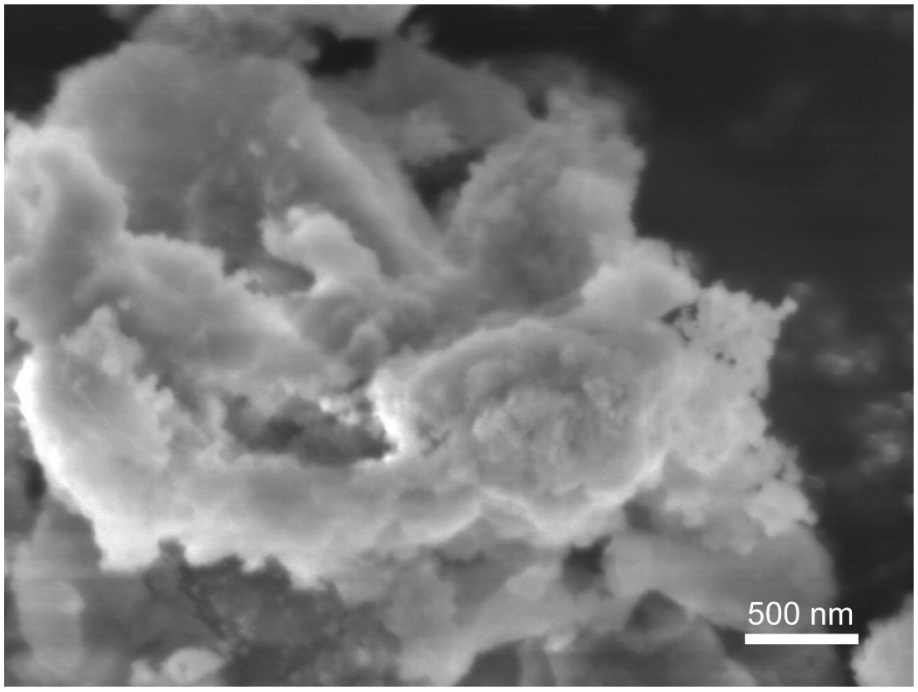

Figure S11. SEM image of as-synthesized Pt-free FeCoNiCu prepared at 0.75 M SBH. Uncontrolled overgrowths and poorly defined porosity features are observed.

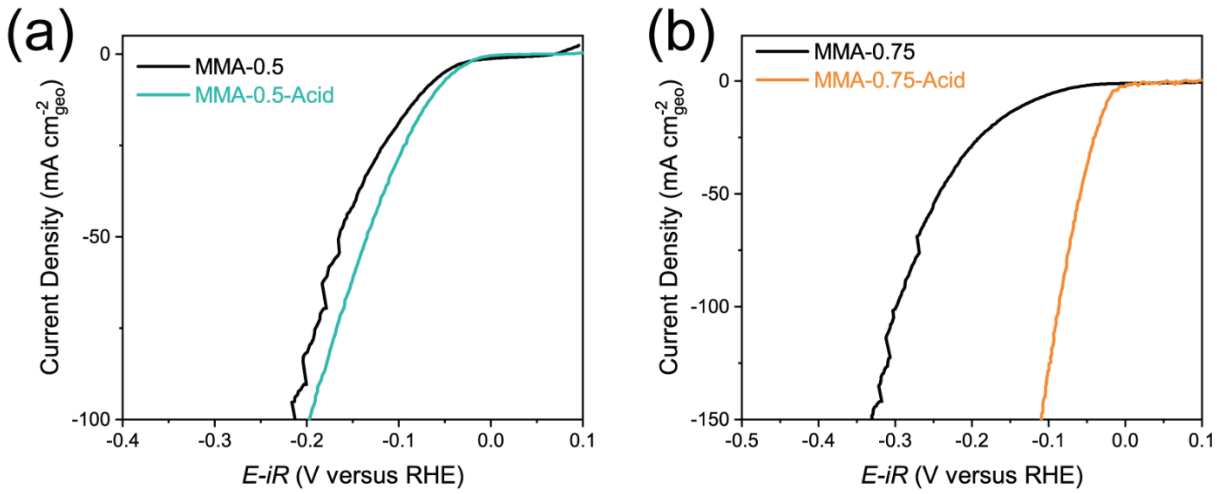

Figure S12. HER polarization curves of (a) as-synthesized MMA-0.5 and MMA-0.5-Acid and (b) as-synthesized MMA-0.75 and MMA-0.75-Acid, measured in 1.0 M KOH.

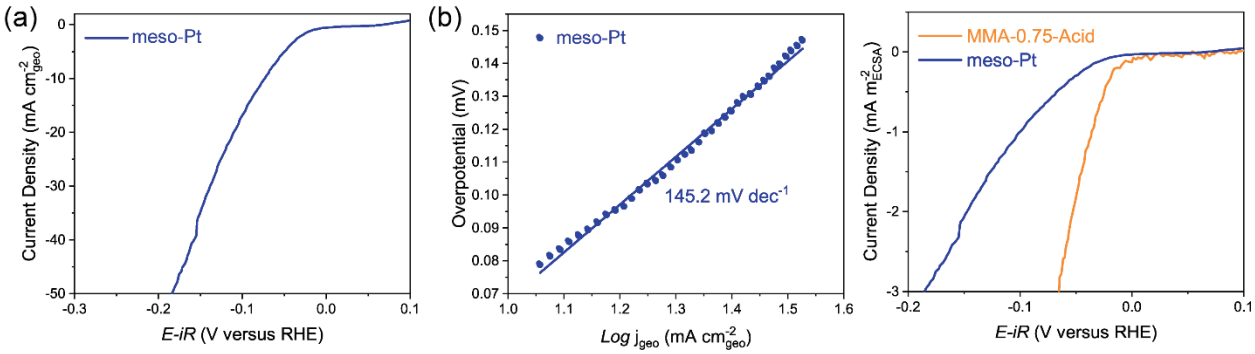

Figure S13. (a) HER polarization curve normalized to geometric electrode area and (b) corresponding Tafel slope of the mesoporous Pt (meso-Pt) control sample, measured in 1.0 M KOH. (c) HER polarization curves of meso-Pt and MMA-0.75-Acid, normalized to electrochemical surface area (ECSA).

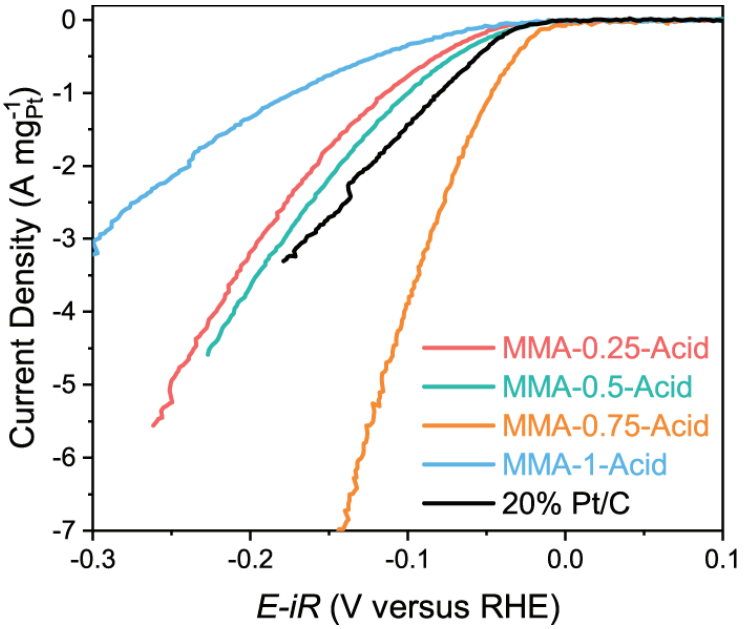

Figure S14. HER polarization curves of acid-treated MMA samples and commercial 20 wt% Pt/C, normalized to Pt mass.

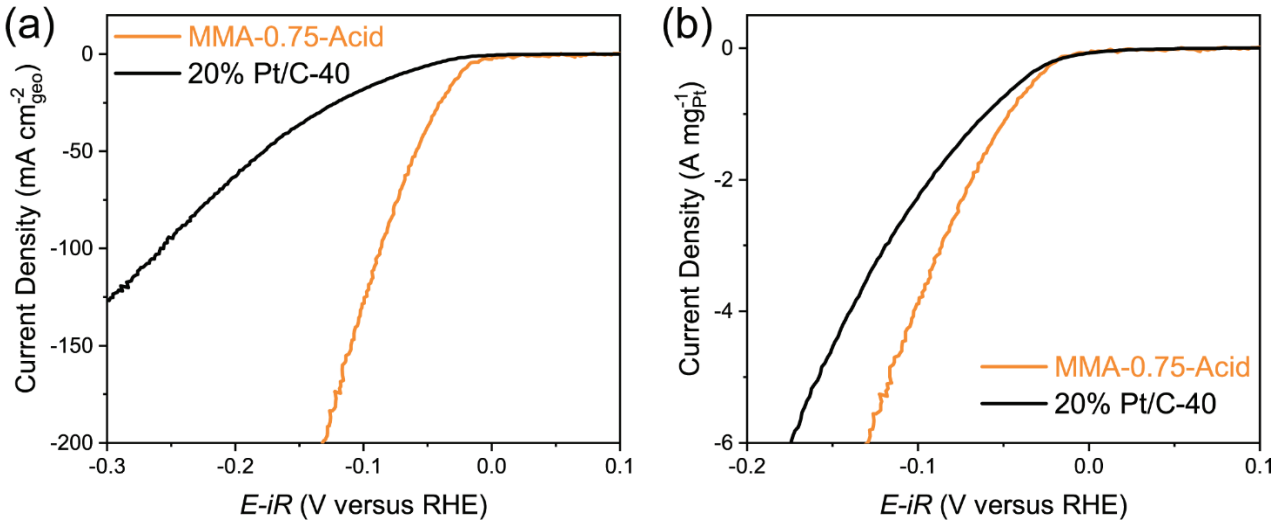

Figure S15. HER polarization curves of commercial 20 wt% Pt/C with a lower dry loading of 40 μg cm^{-2}, corresponding to a Pt loading of ~8 μg$_{Pt}$ cm^{-2}, normalized to (a) geometric electrode area and (b) Pt mass.

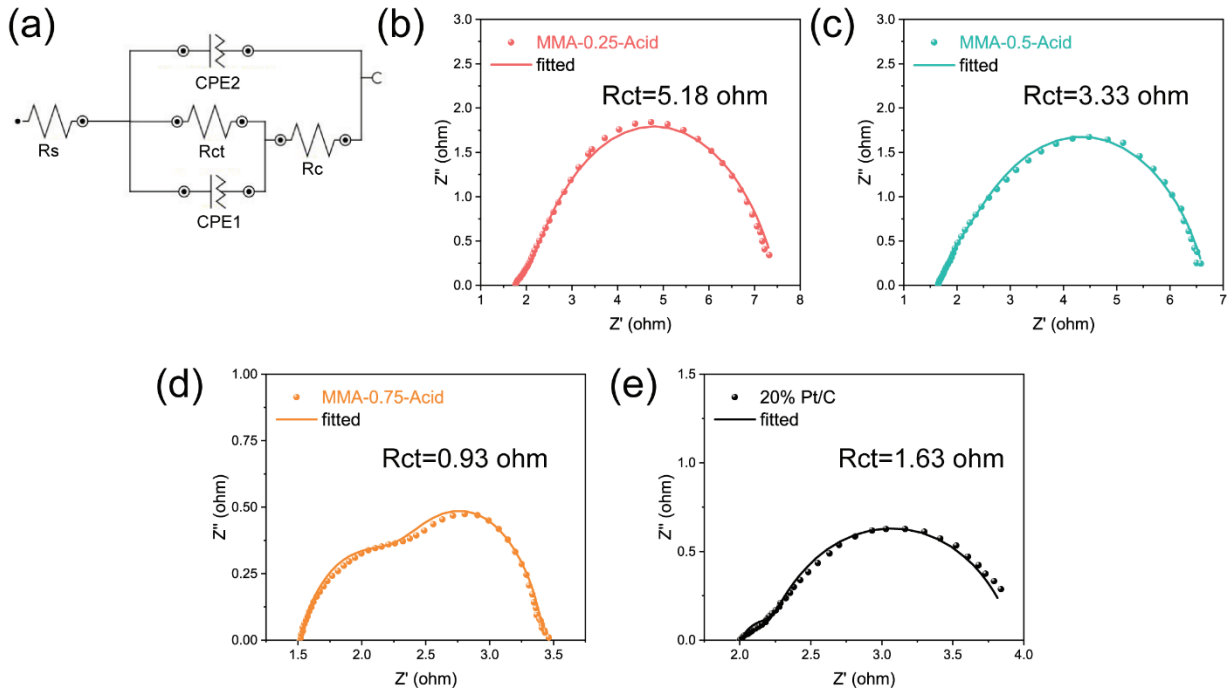

Figure S16. (a) Equivalent circuit used for fitting the Nyquist plots of acid-treated MMA samples. Fitted Nyquist plots and the corresponding extracted charge transfer resistance (R_{ct}) values for (b) MMA-0.25-Acid, (c) MMA-0.5-Acid, (d) MMA-0.75-Acid, and (e) commercial 20 wt% Pt/C.

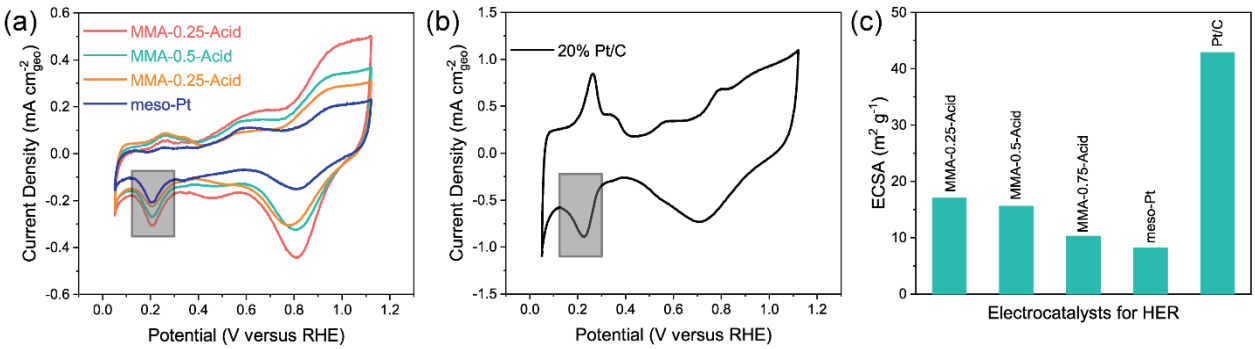

Figure S17. CV plots recorded at a scan rate of 10 mV s^{-1} for (a) acid-treated MMA samples and mesoporous Pt and (b) commercial 20 wt% Pt/C, used for electrochemical surface area (ECSA) determination. The HUPD regions employed for ECSA quantification, corresponding to the potential window of 0.11 to 0.33 V vs RHE, are highlighted by grey rectangles. (c) Bar chart summarizing the ECSA values obtained from HUPD analysis.

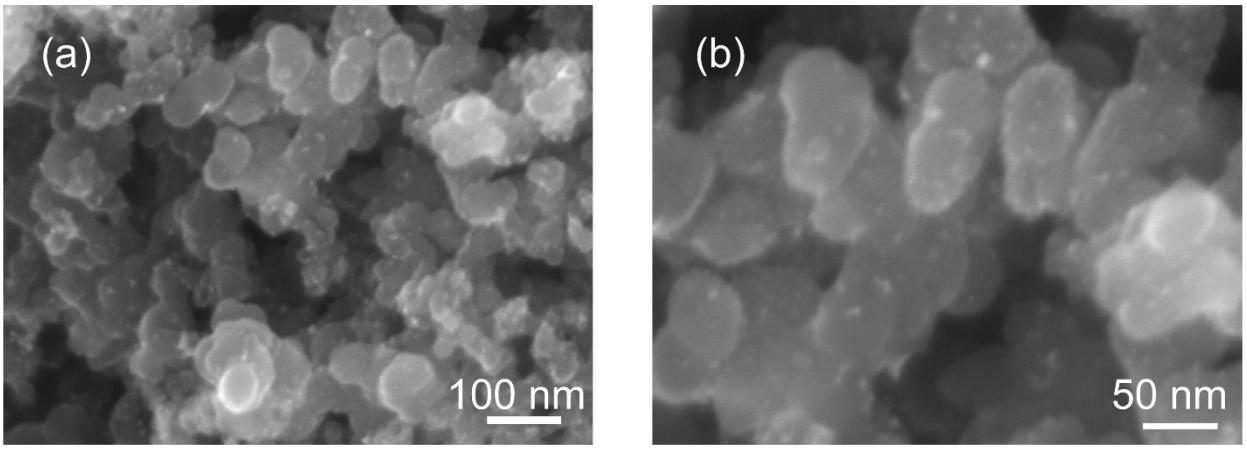

Figure S18. SEM images of commercial 20 wt% Pt/C. The bright spots on the carbon support correspond to Pt nanoparticles. From these SEM images, the average Pt particle size is estimated to be below 10 nm, which results in a higher density of exposed active sites.

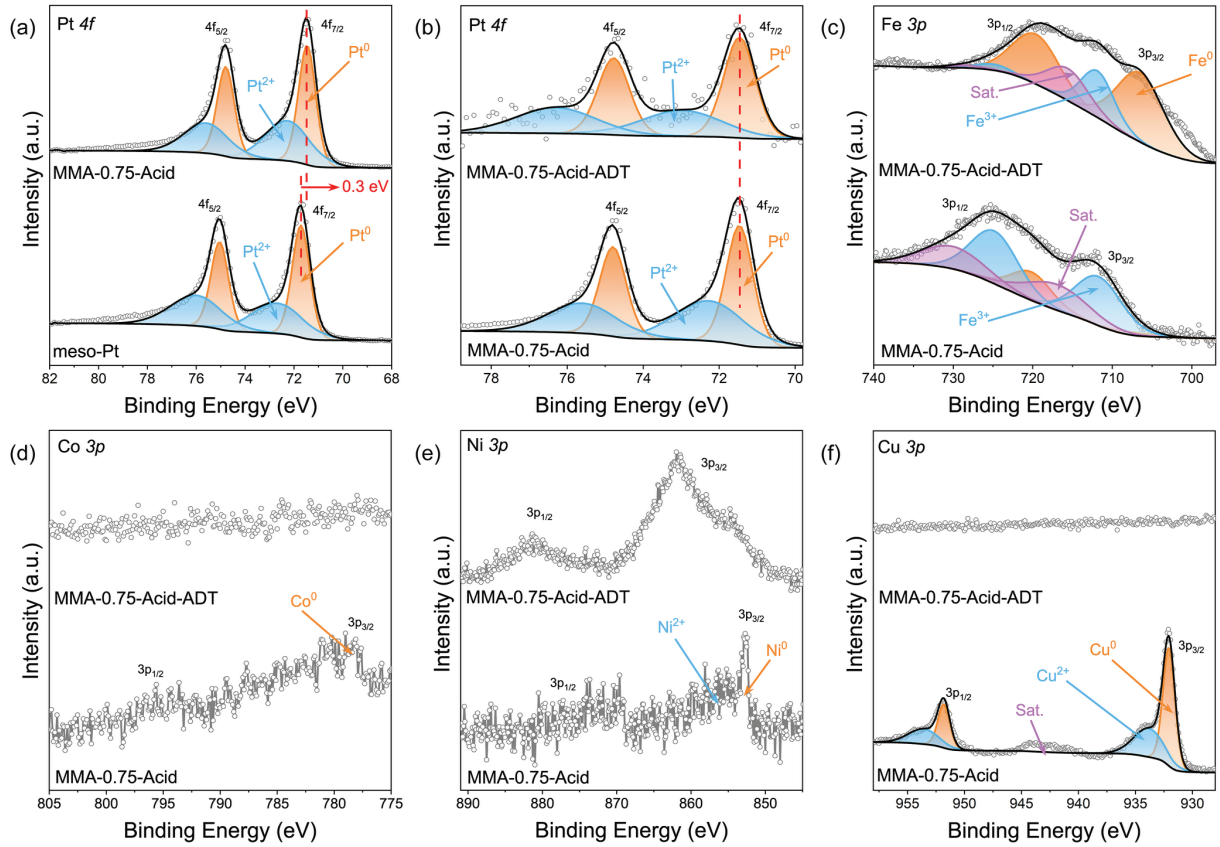

Figure S19. XPS spectra of (a) mesoporous Pt-only (meso-Pt) and MMA-0.75-Acid in the Pt *4f* region, and of MMA-0.75-Acid and MMA-0.75-Acid before cycling and after 100,000 ADT CV cycles for (b) Pt *4f*, (c) Fe *3p*, (d) Co *3p*, (e) Ni *3p*, and (f) Cu *3p*.

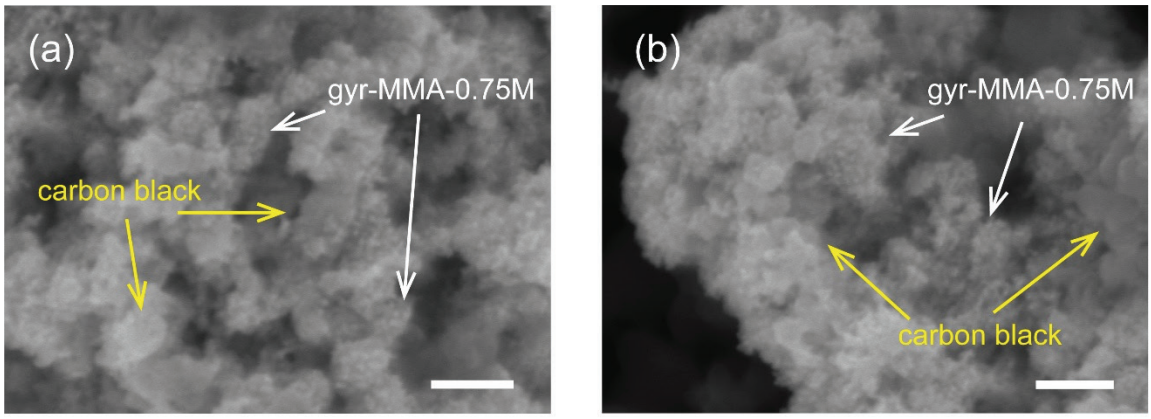

Figure S20. SEM images of MMA-0.75-Acid electrode after 100,000 CV cycles for ADT. All scale bars are 100 nm.

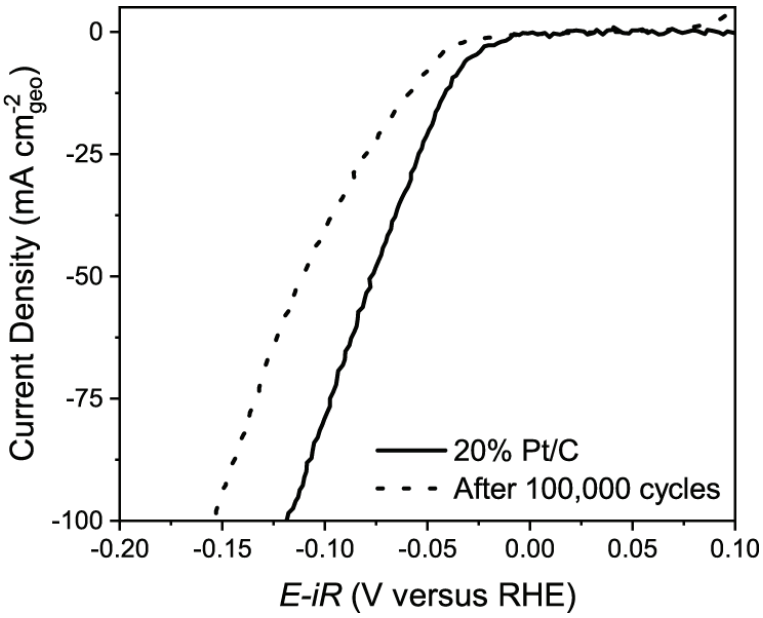

Figure S21. HER polarization curves of commercial 20 wt% Pt/C before and after 100,000 CV cycles for ADT.

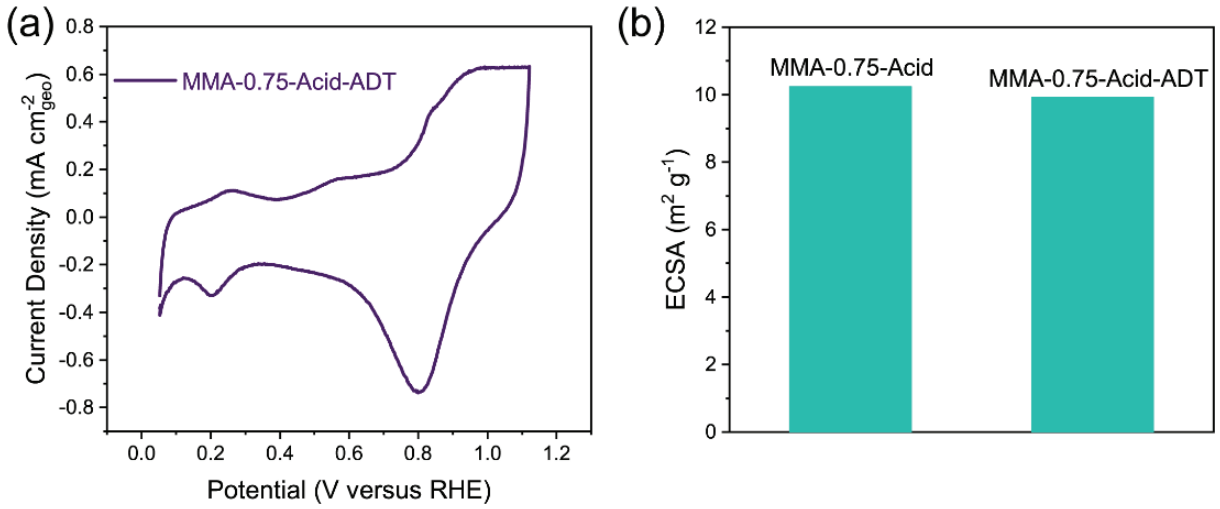

Figure S22. (a) CV of MMA-0.75-Acid after 100000 ADT cycles recorded at a scan rate of 10 mV s^{-1}. (b) ECSA values determined from HUPD.

Table S1. Elemental compositions of MMA samples determined by ICP-OES.

Sample	**Pt/mg L^{-1}**	**Fe/mg L^{-1}**	**Co/mg L^{-1}**	**Ni/mg L^{-1}**	**Cu/mg L^{-1}**
MMA-0.25-Acid	237.51	2.80	N/A	N/A	28.80
MMA-0.5-Acid	152.30	1.90	N/A	N/A	18.66
MMA-0.75	67.91	17.74	18.44	19.09	15.56
MMA-0.75-Acid	224.89	1.36	0.60	0.41	12.92
MMA-1-Acid	201.20	2.02	0.50	0.36	18.31

Table S2. Relative elemental composition ratios of the MMA samples determined by ICP-OES.s

Sample	**Pt/%**	**Fe/%**	**Co/%**	**Ni/%**	**Cu/%**
MMA-0.25-Acid	70.8	2.9	N/A	N/A	26.3
MMA-0.5-Acid	70.4	3.1	N/A	N/A	26.5
MMA-0.75	22.5	20.5	20.2	21	15.8
MMA-0.75-Acid	82.5	1.7	0.7	0.5	14.6
MMA-1-Acid	75.3	2.6	0.6	0.5	21

Table S3. Summary of HER performance of recently reported electrocatalysts in alkaline media. Mass activity is reported in units of amperes per mass of platinum group metals (A m_{PGM}^{-1}).

Catalyst	**Form**	**Overpotential (mV) @10 mA cm^{-2}**	**Mass Activity (A mg_{PGM}^{-1})**	**Ref.**
This work (MMA-0.75-Acid)	ordered mesoporous particles	25	3.9@100 mV 2.1@70 mV	
$PtNi_5$-0.3	nanoparticles	26.8	2.36@70 mV	[1]
PtNi	anisotropic superstructures	27.7	2.80@70 mV	[2]
MI-PtZnCo	mesoporous particles	29	1.77@100 mV	[3]
N-LDH/2D-Pt	nanosheet	31	2.43@100 mV	[4]
c-PtPd@a-NiB	hollow nanopolyhedra	31	0.21@70 mV	[5]
PdPtCuNiP	metallic glass	32	-	[6]
$PtSn_4$	bulk single crystal	37	-	[7]
Disordered PtNi/C	nanoparticles	39.7	1.03@70 mV	[8]
Pt_3Ni_3	nanowires	40	-	[9]
$PtSe_2$/Pt Heterointerface	heterointerface	42	-	[10]
FeCoPdIrPt@GO	nanoparticles	42	3.03@100 mV	[11]
hcp-Pt-Ni	nano-multipods	65	3.03@70 mV	[12]

References

1 C. Zhang, X. Liang, R. Xu, C. Dai, B. Wu, G. Yu, B. Chen, X. Wang and N. Liu, *Adv. Funct. Mater.*, 2021, **31**, 2008298.
2 Z. Zhang, G. Liu, X. Cui, B. Chen, Y. Zhu, Y. Gong, F. Saleem, S. Xi, Y. Du, A. Borgna, Z. Lai, Q. Zhang, B. Li, Y. Zong, Y. Han, L. Gu and H. Zhang, *Adv. Mater.*, 2018, **30**, 1801741.
3 Y. Wang, H. Lv, L. Sun, F. Jia and B. Liu, *Adv. Energy Mater.*, 2022, **12**, 2201478.
4 S. W. Jang, S. Dutta, A. Kumar, Y.-R. Hong, H. Kang, S. Lee, S. Ryu, W. Choi and I. S. Lee, *ACS Nano*, 2020, **14**, 10578–10588.
5 K. Deng, T. Ren, Y. Xu, S. Liu, Z. Dai, Z. Wang, X. Li, L. Wang and H. Wang, *J. Mater. Chem. A*, 2020, **8**, 8927–8933.
6 Z. Jia, K. Nomoto, Q. Wang, C. Kong, L. Sun, L. Zhang, S. Liang, J. Lu and J. J. Kruzic, *Adv. Funct. Mater.*, 2021, **31**, 2101586.
7 G. Li, C. Fu, W. Shi, L. Jiao, J. Wu, Q. Yang, R. Saha, M. E. Kamminga, A. K. Srivastava, E. Liu, A. N. Yazdani, N. Kumar, J. Zhang, G. R. Blake, X. Liu, M. Fahlman, S. Wirth, G. Auffermann, J. Gooth, S. Parkin, V. Madhavan, X. Feng, Y. Sun and C. Felser, *Angew. Chem., Int. Ed.*, 2019, **58**, 13107–13112.
8 H. Chen, G. Wang, T. Gao, Y. Chen, H. Liao, X. Guo, H. Li, R. Liu, M. Dou, S. Nan and Q. He, *J. Phys. Chem. C*, 2020, **124**, 5036–5045.
9 P. Wang, K. Jiang, G. Wang, J. Yao and X. Huang, *Angew. Chem., Int. Ed.*, 2016, **55**, 12859–12863.
10 Z. Wang, B. Xiao, Z. Lin, Y. Xu, Y. Lin, F. Meng, Q. Zhang, L. Gu, B. Fang, S. Guo and W. Zhong, *Angew Chem Int Ed*, 2021, **60**, 23388–23393.
11 S. Gao, S. Hao, Z. Huang, Y. Yuan, S. Han, L. Lei, X. Zhang, R. Shahbazian-Yassar and J. Lu, *Nat. Commun.*, 2020, **11**, 2016.
12 Z. Cao, Q. Chen, J. Zhang, H. Li, Y. Jiang, S. Shen, G. Fu, B. Lu, Z. Xie and L. Zheng, *Nat. Commun.*, 2017, **8**, 15131.